Journal of Hazardous Materials Advances
November 2021, Volume 3, Pages 100009 (12p.)
https://doi.org/10.1016/j.hazadv.2021.100009 https://archimer.ifremer.fr/doc/00720/83182/

Redox-driven geochemical partitioning of metal(loid)s in the iron-rich anoxic sediments of a recently flooded lignite mine pit: Lake Medard, NW Czechia

Umbría-Salinas Karelys [1, *], Valero Astolfo [1, 2], Jan Jiří [1], Borovec Jakub [1, 2], Chrastný Vladislav [3], Petrash Daniel A. [1, 4]

[1] Biology Centre CAS, Soil and Water Research Infrastructure, Na Sádkách 7, 370 05 České Budějovice, Czech Republic
[2] University of South Bohemia, Faculty of Science, Branisovská 1645/31a, 370 05 České Budějovice, Czech Republic
[3] Department of Environmental Geosciences, Faculty of Environmental Sciences, Czech University of Life Sciences Prague, Kamýcká 129, 165 21 Prague 6, Czech Republic
[4] Department of Environmental Geochemistry and Biogeochemistry, Czech Geological Survey, 152 00 Prague 5, Czech Republic

* Corresponding author : Karelys Umbria-Salinas, email address : karelys.umbria@bc.cas.cz

Abstract :

We evaluated the geochemical partitioning of Fe, Mn, As, V, and REE in sediments of a recently flooded open-cast lignite mine to interpret their response to recently established anoxia, and minor variations in the redox potential of its ferruginous bottom water column. Results from a sequential extraction scheme targeting reactive Fe mineral phases are combined with an assessment of sediment enrichment factors and REE systematics. Across the sediment pile metal(loid)s are being released from pre-existing authigenic phases as minor shifts in redox potential induce elemental immobilisation throughout co-precipitation with Fe into mineral phases of diverse reactivity. REE systematics confirms that minor oscillations in the water column's redox state can trigger swift changes in the speciation of the redox-sensitive elements. The observed metal(loid)s enrichment in the sediments can either be considered an ecological risk, if a management scenario involving solely recreational purposes is conceived; but it can also be seen as a feasible source of critical metals (e.g., REE and V) that are amenable to sustainable, secondary metal recovery endeavours. By anticipating the fate of redox-sensitive metal(loid)s in our study site, we provide parameters useful to delineate management programmes of this and similar post-mining lakes.

Graphical abstract

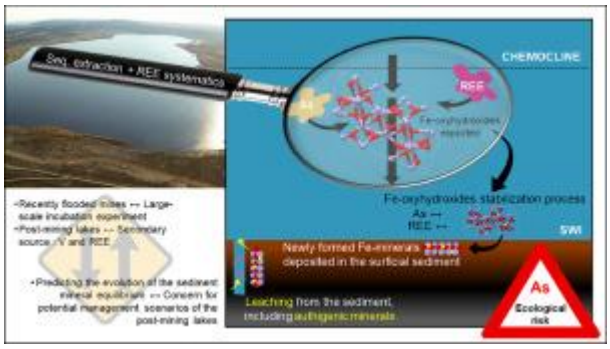

Highlights

► Metal's fate was assessed by coupling their partitioning with REE systematics. ► Highly mobile As(III) would represent a potential ecological risk after holomixis. ► Sediment's REE systematics pinpoint redox state changes in the water column. ► Post-mining lakes could be a secondary sources of valuable transition metals.

Keywords : Elemental-partitioning, meromictic lake, sequential extraction, pit lake, reactive iron

1. Introduction

Post-mining lakes result from water filling of former open-cast mines after mining operations cease (Gammons et al., 2009). Flooding either proceeds artificially (e.g., by deviating nearby river waters for reclamation purposes), or naturally by runoff and groundwater infilling (Schultze et al., 2017). Many coal and lignite mines are now post-mining lakes (Denimal et al., 2005; Schultze et al., 2010; Petrash et al., 2018), and their number is expected to increase as coal mining and coal-powered energy generation are progressively phased out worldwide.

The hydrochemistry of lignite post-mining lakes usually reflects the effects of weathering on Fe-sulphides, Fe-hydrous sulphates, and to a lesser extent aluminosilicate and sometimes carbonate phases comprising the outcropping, coal seam-associated facies and/or the former mine spoils (Denimal et al., 2005; Schultze et al., 2010). In their early stage, which could last up to 100 yrs., post-mining lakes tend to be meromictic since density stratification between upper and bottom waters prevents the seasonal mixing of the water column (Boehrer & Schultze, 2008; Schultze et al., 2010). Density stratification generates a permanent chemical boundary zone, known as the chemocline, that separates an oxygenated and seasonally mixed mixolimnion (upper waters) from an anoxic monimolimnion (Boehrer & Schultze, 2008). The chemocline exhibits marked activity gradients of redox-sensitive elements (Sánchez-España et al., 2020).

Post-mining lakes can slowly evolve towards holomictic conditions (Schutlze et al., 2010) which is followed by the solubilisation of high loads of potentially toxic metalloids - such as As - from the Fe(III)-oxyhydroxides that often comprise their sediments (Azcue & Nriagu, 1993; Tabelin et al., 2020). The leaching of potentially toxic metal(loid)s is probably the greatest impediment against efforts to develop complex ecological networks that could allocate a safe use of these sites for recreational purposes (e.g., Otchere et al., 2004; Brázová et al., 2021).

Conversely, controlled scavenging of critical transition metals such as rare earth elements (REE) from the redox stratified water column, for example through emerging methods for secondary biotechnological recovery (Thompson et al., 2017; Hua et al., 2019), would secure a supply of these metals. Establishing post-mining lakes as a secondary source of valuable trace metals would be crucial to a circular economic model for the redevelopment of coal-mining districts in countries such as Australia, Czech Republic, Germany, and Poland, among others with a heavy economic reliance in coal.

Despite their relevance, there is a lack of studies showing how short-term development of contrasting physicochemical conditions in the water column of recent post-mining lakes affects the solid-state geochemical partitioning of metal(loid)s. Anticipating the fate of metals as drastic changes of the bottom water column's redox state proceed is of concern for the managing scenarios of post-mining lakes (e.g., Jakob-Tatapu et al., 2021; Woon et al., 2021).

Here we examine depth variations in the concentrations and redox behaviour of Fe, Mn, As, REE, and V in recent lacustrine sediments collected from a former open-cast lignite mine that was flooded between 2008 and 2015 (Lake Medard, NW Czech Republic). This recently flooded post-mining lake features oligotrophic and meromictic conditions, and an enrichment in dissolved SO_4^{-2}, Fe(II), and other metal(loid)s in its bottom water column (Petrash et al., 2018). At the sediment-water interface (SWI), Fe-oxyhydroxides formed at the chemocline have accumlated together with weathered minerals derived from a carbonate-rich Miocene claystone (Petrash et al., 2018).

To assess the response of Lake Medard sediments to the recently established bottom water anoxia, we evaluated the short-term geochemical partitioning of redox-sensitive metal(loid)s into reactive Fe minerals that occur to a depth of 18 cm in the sediment pile. Arsenic

was selected as a proxy for the fate of redox-sensitive pollutants of concern; Mn was considered to better assess the redox behaviour of Fe, whilst V and REE were evaluated as proxies for economically valuable critical transition metal recovery.

We coupled a sequential extraction protocol that targeted Fe mineral phases with diverse crystallinity and redox reactivity (e.g., ferrihydrite, lepidocrocite, goethite, and siderite), with Enrichment Factor (EF) and REE systematics (e.g., Bau & Möller, 1993). The approach applied here permits anticipating the redox dynamics of the metals of interest over potential variations of physicochemical parameters. Therefore, results from this research could be applied to improve the decision-making process of remediation and/or management programmes of post-mining lakes featuring similar hydrochemical and geological contexts.

2. Methods

2.1. Study area

Lake Medard (50°10′45″N, 12°35′45″E) is an engineered oligotrophic lake located in the Karlovy Vary region (NW Czech Republic; Figure 1). It was formed by the flooding of a former open-cast lignite mine – known as Medard-Libík – with water from the nearby Ohře river between 2008 and 2015. It has an elongate surface area of *ca.* 4.93 km^2, with maximum central and eastern water column depths of *ca.* 60 m. Currently, the lake receives influx from an acidic surface drainage (Jozef creek; hereafter referred to as JC) that is rich in sulphate (SO_4^{2-}), Fe(II), and other metals (Petrash et al., 2018). After water infilling, continuous hydrochemical monitoring of key physicochemical parameters (i.e., dissolved oxygen, Eh, pH, conductivity, and temperature) of the newly formed oligotrophic lacustrine system has consistently shown the establishment of meromictic conditions. Accordingly, the bottom water column features a dysoxic hypolimnion and an anoxic ferruginous monimolimnion ([Fe(II)]= 127 ± 17 μM), with

high dissolved SO_4^{-2} (19 ± 2 mM) but low dissolved hydrogen sulphide concentrations (<0.3 μM; Petrash et al., 2018).

2.2. Sample Collection

Two undisturbed sediment cores were retrieved from the lake bottom at *ca.* 55 m depth in its central area. The sampling campaigns were carried out in November 2019 (S_1), and December 2020 (S_2). Before sediment sampling, was measured the conductivity, pH, Eh, dissolved oxygen (O_2), and temperature of the bottom water column from 50 m depth down to about 1 m above the anoxic SWI. Also, the bottom water column (monimolimnion, 50 to 56 m), and the Jozef creek waters were sampled. At the lab, the core slicing was performed at 2 cm resolution and up to 18 cm depth (S_1) and 8cm (S_2). For further details see Supplementary Material 1 (Appendix A, SM1.1).

2.3. Powder X-ray diffraction analysis

The mineralogy of the sediments was determined by a powder diffractometer (D8 ADVANCE, Bruker) equipped with a CuKα anode, using a 2Θ range of 4-80°, a step size of 0.015°, and a count time of 0.8 s /step. Semi-quantitative phase analysis was performed following the Rietveld method (Post & Bish, 1989). See Appendix A, SM1.2 for further details.

2.4. Chemical analyses

2.4.1. Organic matter, total organic carbon, total nitrogen, and total sulphur content determination

Sediment aliquots (100 mg) were digested using cold 10 % HCl for 24 h to dissolve the carbonate fractions, before determining the total organic carbon (TOC) and nitrogen (TN) contents using a CHNS/O elemental analyser (Flash Smart, Thermo Fisher Scientific). Variability

of the elemental concentration data obtained was between 0.21 and 0.37 % for TOC, and 0.02 to 0.05 % for TN, based on repeated analyses (n = 12) of the stream sediment certified reference material STDS-1 (Canadian Centre for Mineral and Energy Technology) and the peat soil standard SC2351 (Sercon).

2.4.2. Trace metals and rare earth elements content determination

Based on the obtained mineralogical data, we applied a modified sequential extraction scheme that was aimed at dissolving Fe-bearing mineral phases of variable redox reactivity (e.g., Poulton & Canfield, 2005; Claff et al., 2010). Sediment aliquots (100 mg), corresponding to each of the sub-sampled depths, were chemically leached (10 mL of each of the extractants) to determine the geochemical partitioning – exchangeable metallic cations (M_{EX}), metals bonded to carbonate minerals (M_{CARB}), bonded to easily reducible Fe-oxyhydroxides (M_{ERO}), and bonded to reducible and highly crystalline Fe-oxyhydroxides (M_{RO}) – of Fe, Mn, V, As, and REE in the sediment pile. The metals extracted by the applied sequential scheme are bound to the highly redox-reactive Fe pool of the sediments (i.e., after Poulton & Canfield, 2005). As such, any residual iron-binding phases most likely comprised of silicates, can be regarded as unreactive towards dissolved sulphide on the time scales encountered in post-mining lake sediments (Canfield et al., 1992; Raiswell & Canfield, 1996). Details on the sequential extraction scheme are provided in the Appendix A, SM1.3.

Each of the extracts was analysed for metal(loid)s (Al, Fe, Mn, V, and As), and REE (La, Ce, Pr, Nd, Sm, Eu, Gd, Tb, Dy, Ho, Er, Tm, and Yb) concentrations via quadrupole inductively coupled plasma mass spectrometry (Xseries II, Thermo Scientific) at the Czech University of Life Sciences, Prague. As an internal standard, we used ^{115}In at 1 µg L^{-1} concentration. Also, to achieve optimal analytical conditions for REE, the instrument was tuned to reach a CeO/Ce ratio

<1.5 %. A five-point calibration curve was performed by using dilutions of single-element standards for ICP (Certipur®) and REE mix for ICP-MS (TraceCERT®) with concentrations of 0, 1, 10, 20, and 50 µg L^{-1}. The variability of the elemental concentration data was less than 10 %. This is based on analyses of replicates (n = 3) for each extractant and element.

The water sample concentrations of the same elements listed above were determined by using High-Resolution ICP-MS (Thermo Scientific Element2) at the Pôle Spectrométrie Océan in Brest, France. The instrument was tuned to minimize oxide production, and mixed mono-elemental Pr-Nd, Ba-Ce, and Sm-Tb solutions were analysed to quantify potential oxide interferences prior to the analyses, which were negligible. Calibration was performed against multi-element solutions and analysed in the same session as unknowns to monitor accuracy (better than 5 % for REE, and 10 % for the other elements of interest).

2.5. Data treatment

2.5.1. Metal enrichment determinations

For assessing differential accumulation of the metal(loid)s in the lake sediment profiles examined here, we estimated the Enrichments Factors (EFs; Appendix A, SM1.4), considering the total concentrations (bulk extractable pool) and discrete background values of relevance (e.g., Dendievel et al., 2020). These background values included the metal content of world average shale (WAS) and carbonate (WAC) (Turekian & Wedepohl, 1961), and concentrations reported for the claystone lithology of the Sokolov basin (i.e., Miocene Cypris Fm.; Kříbek et al. 1998), which is the source of detrital material that accumulated in the abandoned lignite mine prior to and during flooding. By evaluating the respective extractant concentrations with regard to the former background values, we estimated the relative sediment enrichment/depletion in the Fe-oxyhydroxides (M_{ERO} + M_{RO}) and carbonate (M_{CARB}) fractions.

To obtain a broader estimation on whether a redox-sensitive metal(loid) of interest is significantly enriched in our post-mining lacustrine sediment profiles, we evaluated the obtained dataset using average elemental concentrations of the overlying O_2-depleted water column (50 to 55 m depth; Appendix A, ST1) to calculate relative enrichments. Besides, we also evaluated the sediment's relative enrichment by using elemental concentrations of the surficial Jozef creek water (Figure 3b). JC is thought representative of the hydrochemistry of the mine's runoff waters before flooding of the former mine. It is used primarily as a reference to the aqueous elemental partitioning that would have governed mineralisation reactions that occurred in the sediments prior to flooding of the pit and the establishment of the now anoxic sediment-water interface. Details on the mineralogy that was in equilibrium with the mining-impacted water bodies (prior to river water infilling) are available in Murad & Rojík (2003; 2005).

2.5.2. Rare earth elements anomalies and fractionation

Rare earth elements anomalies (i.e., relative enrichment regarding selected neighbouring elements within the group) were calculated (Eqs. 2 and 3, Appendix A, SM1.5) to distinguish the geochemical behaviour of lanthanides that could reflect variations in environmental redox conditions in the sediment profile (Shields & Stille, 2001; Hannigan et al., 2010). See Appendix A, SM1.5 for further details. Besides, the REE fractionation degree (i.e., light REE *vs.* heavy REE) was calculated by following Nance & Taylor (1976; Eq. 4, Appendix A, SM1.5).

2.5.3. Statistical analyses

Normality of data distribution was evaluated by the Shapiro-Wilk test at the 95 % significance level. When necessary, i.e., for elements exhibiting relatively low concentrations, data were plotted using a log-scale. Statistically relevant differences were evaluated by the t-test ($p < 0.05$) – for each fraction and total (bulk) and considering the two sampling periods. Data processing was performed with the software R Foundation for Statistical Computing (Vienna, Austria; R Core Team, 2016).

2.5.4. Potential metal(loid) release from the reactive sediments

By using the average elemental concentrations, the sediment characteristics (e.g., density and porosity), and the area of Lake Medard where O_2-depleted conditions are prevalent (Figure 1) we estimated the potential of the reactive mineral phases to release As, V, and REE from the sediment pile until 8 cm. The utilised considerations are described in Appendix A, SM1.6. This approach also allowed us to determine the potential concentrations of metal(loid)s that would establish in the monimolimniom as a latent source of pollution or as an economically feasible resource of critical metals.

3. Results and discussion

3.1. Sediment-water interface characterisation

The pH values in both sampling periods, S_1 and S_2, displayed only minor variability. Despite the lack of mixing, the Eh of the monimolimnion increased by S_2 *vs.* S_1 (i.e., -80 *vs.* -192 mV, respectively). This change in redox potential was consistent with a shift in the depth of the chemocline to 52 m (S_2) from 48 m depth (S_1). Such a shift is interpreted to be linked to less groundwater recharge as the three months preceding our 2020 sampling (S_2), were on average, considerably drier than the previous year, when S_1 took place (i.e., 77 % less precipitation according to the records of the Czech Meteorological Institute, 2021). Less precipitation before S_2 diminished the recharge of salts dissolved by fluid-rock interaction in the bedrock and underlying crystalline lithologies, which are known to host epithermal fracture mineralisation (Pačes & Šmejkal, 2004). Decreased dissolution of subsurface salts caused the monimolimnion waters to become less dense. In turn, this triggered an increase in the depth of the mixolimnion and shifted the chemocline (e.g., Boehrer & Schultze, 2006). Consistent with this interpretation there was a decrease in the monimolimnion's conductivity from 6,808 µS cm^{-1} during S_1 to 2,607 µS cm^{-1} during S_2. A more recent hydrochemical monitoring of the water column (early May 2021) showed that such conditions, however, were short-lived as redox parameters resembling S_1 were re-established only five months after S_2 (Appendix A, ST2).

Despite the increase in the redox potential of the monimolimnion during S_2, during both periods the bottom sediments remained under oxygen-depleted conditions and the overlaying waters displayed dissolved O_2 concentrations between 0.1 and 1.4 mg L^{-1}. XRD analyses (Appendix A, SF1) of the sediments showed that rutile (TiO_2), siderite ($FeCO_3$), gypsum ($CaSO_4.2H_2O$), and in lower abundance pyrite (FeS_2) are dominant phases within a clayey sediment matrix that is composed mainly of kaolinite (Table 1).

FeOOH polymorphs (i.e., lepidocrocite and goethite) have accumulated as heterogeneous mineral clusters embedded in an organic clay-rich matrix. Amorphous precursors to these authigenic Fe(III) mineral phases are formed at the chemocline; from where they are exported to the anoxic SWI and stablise (Petrash et al., 2018). Underlying the recent sediments are detrital materials derived from weathered claystone (Cypris Fm.; Kříbek et al., 1998). These sediments also contained a secondary, mine-drainage precipitated mineralogy, including jarosite ($Fe_3(SO_4)_2(OH)_6$), which occurred at more acidic spring sources; also schwertmannite ($XFe_8O_8(OH)_6SO_4$), ferrihydrite, and goethite (Murad & Rojík, 2003; 2005). The oxyhydroxysulfate phases likely behaved as powerful scavengers for As(III) in solution leading to As(III)-enriched precipitates (Paikaray et al., 2017). When we compared our XRD analyses (Appendix A, SF1) with previously reported diffraction data of pit lake sediments (Murad & Rojík, 2003; 2005), it could be observed that the oxyhydroxysulphates have undergone complete dissolution under the physicochemical conditions governing the anoxic deep water/ sediments examined here, thus releasing both As and sulphate. Their alteration products (i.e., the Fe-oxyhydroxides polymorphs) exhibit contrasting crystallinities and presumably much lower redox reactivities towards As (Park et al., 2018), and, as discussed below, occur at variable abundances in the now ferruginous sediment pile.

The total organic carbon and total nitrogen contents were higher in the uppermost layer (0-2 cm) and decreased towards the bottom (Table 1). In detail, the C:N ratio ranged from 16 to 30 from 0 to 8 cm, and below this section ranged between 34 and 86 (by S_1). These results indicate that N has accumulated in the upper sediments following flooding, and despite the lake's current oligotrophic nature (Vejřík et al., 2017). A significant downcore increase in the C:N ratio reveals

depletion of N in the lower sediment organic reservoir and reflects an increase in the proportion of refractory OC derived from lignite.

3.2. Trace metals fractionation in surface sediments

Table 2 shows the total concentration at each depth for each of the elements extracted in our four sequential steps for both sampling periods. We refer hereafter to these total concentration values as the highly reactive pool of any given metal (M_{HR}), and are used for normalisation purposes as well as for enrichment factors calculations (Appendix A, SM1.4). The Al_{HR} pool, and Fe_{HR} increased with increasing depth (Table 2). At the 8 cm depth, however, an abrupt change in the prevailing trends occurred, and Al_{HR} and Fe_{HR} decreased two- and four-fold, respectively. On the other hand, compared with S_1, Mn_{HR} increased two-fold (to reach 809.2 mg kg^{-1}) by S_2 between 0-2 cm and 4-6 cm, although it must also be noted that this parameter shows a decreasing downcore trend both in S_1 and S_2. The As_{HR} and V_{HR} peaked at the 6-8 cm depth interval, whereas the summatory of all the lanthanides (∑REE) also increased with increasing depth in both periods (Table 2). Below we summarise and compare the partitioning trends of the elements under consideration.

3.2.1. Iron

Fe partitioning in S_1 was principally controlled by easily reducible Fe-oxyhydroxides fraction (Fe_{ERO}), which accounted for 22.0 to 70.1 % of the Fe_{HR} pool (Appendix A, SF2a) and displayed a higher abundance below 10 cm depth. Conversely, in the core collected in S_2 the total Fe_{HR} was principally related to carbonates fraction (Fe_{CARB}), which ranged from 44.8 to 53.8 %. Despite changes in the Fe reactivity trends in S_1 when compared to S_2, only exchangeable Fe (Fe_{EX}) showed a significant difference ($p > 0.05$) between both sampling periods. This is thought to be related to enhanced reductive dissolution of Fe(III)-oxyhydroxides in the S_1 period, which

released additional dissolved Fe(II) (Nealson et al., 2002). Throughout its reoxidation and subsequent precipitation as newly formed poorly crystalline Fe-oxyhydroxides, Fe(II) solubilised from the Fe_{EX} fraction as a response to slight variations in the physicochemical conditions of the water column, contributes significantly to the internal (bottom water) Fe-cycling (Davison, 1993; Nealson et al., 2002).

3.2.2. Manganese

The summatory of Mn_{EX}, Mn_{CARB}, and Mn_{ERO} represented from 84.2 to 93.3 % of the total Mn_{HR} pool in S_1 samples, whereas Mn_{RO} accounted for only 6.7 to 15.8 % (Appendix A, SF2b). Our results indicate that at the top the core, the Mn_{HR} is mostly comprised of the more reactive (weakly bonded) fraction, while downcore it appears to rather be bonded to less reactive phases. This suggests that, at the SWI, Mn could be readily available to be utilised as an alternative terminal electron acceptor to further fuel Fe(III)-based anaerobic microbial respiration pathways (Davison, 1993; Nealson et al., 2002). These pathways may in turn lead to subsequent stabilisation of Fe(II,III)-oxyhydroxides, and induce the co-precipitation of V, As, and REE (Sundman et al., 2020; Kontny et al., 2021). By S_2, the Mn_{HR} pool was found to have increased two-fold (Table 2), and all of the assessed fractions, except for Mn_{EX}, exhibited statistically significant differences ($p < 0.05$) with regard to S_1. The Mn_{HR} pool was then dominated by Mn_{CARB}, which accounted for up to 79.8 % of the total Mn extracted (Appendix A, SF2b), and it showed even higher values at the top of the sediment pile.

3.2.3. Vanadium

Partitioning of V was variable along the sediment profile. In S_1, the summatory of V_{ERO} (81.0 %) and V_{RO} (16.7 %) represented up to 97.7 % of the V_{HR} pool at the top (Appendix A, SF2c). V_{ERO} decreased downcore, but a marked abundance peak is observed between 6 to 10 cm.

The V_{CARB} fraction was not detected in the SWI. Analogously, in S_2, V was mostly bonded to Fe-oxyhydroxides of diverse crystallinity, which together accounted for 97.9 % of the V_{HR} pool. However, in S_2 the V content bound to reducible, more crystalline Fe-oxyhydroxides increased up to 20-fold throughout the entire sedimentary profile, when compared to the first sampling. Thus, the V_{RO} fraction exhibited significant differences between periods ($p < 0.05$).

3.2.4. Arsenic

As partitioned quite differently downcore when compared to the other elements with siderophile affinity also evaluated here (Appendix A, SF2d). In the S_1 period, at the SWI As bonded to easily reducible and highly crystalline Fe-oxyhydroxides, accounting for up to 83.4 % of As_{HR} pool. However, the element was principally bound to As_{RO}, with concentrations ranged between 30.8 and 45.0 % from the top of the core to 8 cm depth. Below this depth, As was dominated by the exchangeable fraction, which displayed increasing downcore concentrations from 39.8 % at 8 cm to 71.8 % at the bottom. In our second sampling, As was principally associated with As_{ERO} fraction, which bound 61.5 to 79.9 % of the As_{HR}, and displayed peak concentrations at the 4-6 cm interval. The As_{CARB} decreased from 38.5 to 3.4 % with increasing depth. Besides, As_{EX} and As_{RO} concentrations were mostly below the detection limit (<DL). Despite the described variations in the As reactivity trends, this element did not show significant differences ($p > 0.05$) between sampling periods in any of the assessed fractions. However, given that As_{EX} was <D.L in the second sampling, we infer that highly mobile As co-precipitated with Fe into the dominant Fe(II,III)-oxyhydroxide and, to a lower extent, carbonate phases.

3.2.5. Rare earth elements

Figure 2e shows the geochemical partitioning of REE. In our S_1 sampling, REE_{ERO} and REE_{RO} fractions accounted for between 53.3 and 99.6 % of the REE_{HR}, respectively (Appendix

A, SF2e). In contrast, REE bound to carbonates dominated the sediment's REE pool by S_2, when this fraction accounted for 47.8 to 52.9 % of the REE_{HR}. Also in S_2 the REE_{RO} represented < 5.0 % of the highly reactive pool. Thus, as described for As above, lanthanides were released after dissolution of easily reducible Fe-oxyhydroxides, and then, trapped within newly formed crystalline Fe-bearing mineral phases (e.g., Hua et al., 2019).

3.2.6. Trace metals remobilisation in the sediment pile

Overall, the geochemical partitioning of the studied elements (Appendix A, SF3) allowed us to determine that at the SWI (0-2 cm), the Fe, V, As, REE, and Mn were principally related to poorly crystalline reducible Fe-oxyhydroxides and to a lesser extent to crystalline phases. Differently to other metals, Mn and As were also weakly sorbed onto the surfaces of discrete Fe-bearing mineral phases (i.e., M_{EX} fraction). From 2 to 8 cm, siderite exerts a more significant role controlling the fate of REE and Mn. This assumption is based on our XDR analyses, which showed the siderite as the only detectable carbonate mineral (2.0-3.0 wt. %). The control exerted by this phase over REE and Mn appears to intensify when slight variations in the environmental redox state occur, such as observed by S_2, when the proportion of metals bonded to carbonate increased substantially. This was also the case for As, which seems to rapidly adsorb onto the surfaces of the Fe-bearing carbonate as a response to dysoxic conditions in the SWI (i.e., S_2).

Below 8 cm, Fe, Mn, REE, and to a lesser degree the V contents appears to be strongly controlled by Fe-oxyhydroxides transformations, whereas As continues to be mostly weakly bonded onto mineral surfaces (Appendix A, SF3). This As behaviour is not surprising given that its oxyanions – arsenate and arsenite – easily adsorb onto reducible oxyhydroxides (Dixit & Hering, 2003), carbonates (Wang et al., 2021), and/or green rust (Perez et al., 2021). Despite variations in the geochemical partitioning trends of the metal(loid)s under examination, the bulk

sediment M_{HR} pool did not present significant differences between sampling periods ($p > 0.05$). Therefore, we infer that the slight variation in the redox state of the overlying water column that we registered by S_2 and S_1 (i.e., -80 and -192 mV, respectively), is sufficient to trigger the release of redox-sensitive metals from the sediment reactive mineral phases (see Zhang et al., 2014). For most metals, this release is followed by their subsequent co-precipitation with Fe either into poorly crystalline oxyhydroxide or recrystallised carbonates. To shed further light on the mobility and partitioning of the metals of interest, in the following section we considered their bulk *vs.* fraction specific enrichment trends.

3.3. Trace metals enrichment

The calculated enrichment factors are displayed in Figure 3. Except for Mn, Ce, and Ho, most elements showed relative enrichment when the carbonate and the combined Fe-oxyhydroxide fractions are compared to world average carbonate (WAC) and shale (WAS) (Figure 3a). Regarding Fe, its EF values (EF_{Fe}) ranged from 5 to 10, indicating acute enrichment with regard to all of the background values. Conversely, the EF_{Mn} only shows acute enrichment when normalised with regard to the Sokolov claystone. V could either be moderately (WAC and Sokolov claystone) or acutely enriched (WAS). The ∑REE in the carbonate fraction, as Mn, did not display enrichment (WAC), but the combined oxyhydroxide pool and the bulk sediments are acutely enriched when compared to both WAS and the Sokolov claystone (Figure 3a). Lastly, As displayed a quite acute enrichment according to all backgrounds as its EF values ranged between 30 and 55. The EF values for the fractions that dominated the geochemical partitioning of the metals – i.e., carbonates and Fe-oxyhydroxides – are summarised in Appendix A, ST3.

When compared the Fe-oxyhydroxide phases to WAS, all metals presented EF values equivalent to those calculated using the M_{HR} pool, except for Mn that showed higher EFs.

Contrastingly, higher EF values regarding WAC are observed for all of the metals under consideration, with As showing the most acute enrichment. In addition, V and the lanthanides revealed higher values downcore for both fractions, whereas EF values for Fe_{CARB}, Mn_{CARB}, and As_{CARB} were higher at the top the sediment core. These data suggest that effectively, Fe-bearing carbonates and Fe-oxyhydroxides of diverse crystallinity re-immobilise redox-reactive metal(loid)s in the most recent lacustrine sediments (i.e., above 8 cm). Some of these metal(loid)s are likely being leached and sourced from alteration products of the former mine bedrock (below 8 cm depth), from where they can diffuse upwards to the now anoxic lake's floor. Also, groundwater inflow carrying dissolution products may be important, as reported in other lignite post-mining lakes (e.g., Denimal et al., 2005). Accordingly, it is plausible that groundwater replenishment causes the bottom water column to exhibit variable conductivities but a prevalent circumneutral pH (~7.2) despite its rather high sulphate contents, which contrasts with what has been observed in acidic post-mining lakes not affected by carbonate dissolution and groundwater influx (cf. Schultze et al., 2010). Finally, the EF_{Fe}, EF_{Mn}, and EF_{V} were higher in S_2 than in S_1 cores, while the EF_{As} and $EF_{\sum REE}$ were lower in the second sampling (Appendix A, ST4). This result confirms that slight Eh variations (i.e., from anoxic to dysoxic conditions) of the SWI, can lead to mineral transformations that allocate remobilisation of Fe and Mn, triggering the release of As, V, and lanthanides.

3.4. Potential lake management scenarios

Due to the metal-polluted nature of the lacustrine sediment under examination, in this section we assess the potential of the reactive mineral phases to release As and accumulate V and REE. Also, by using equilibrium modelling generated by the Geochemist's Workbench™

software as supporting information (Bethke et al., 2021; Appendix A, SF4 and SF5), we speculate on how these latent metal loads would alter the hydrochemistry of the bottom waters.

3.4.1 Latent sediment metal accumulations: As pollution as environmental risk

Regarding As, we estimate that the recent sediments, to a depth of 8 cm, have accumulated between 22.9 and 45.5 mg kg^{-1} of this element; mostly into the more reactive binding phases (i.e., As_{EX} and As_{ERO}). The current sinks of As could change, however, since meromictic post-mining lakes that have sulphate-rich waters, such as Lake Medard, could transition towards an euxinic (i.e., free dissolved hydrogen sulphide) condition (Meyer & Kump, 2008, van de Velde et al., 2021). The establishment of euxinia in the bottom water column would induce As(III) immobilisation through its co-precipitation with Fe(II) into (arseno)pyrite (Telfeyan et al., 2017; Appendix A, SF4 and SF5). Yet, the stabilisation of pyrite from metastable mackinawite (FeS)-like precursors appears to be at present hindered by the general lack of labile organic matter in the oligotrophic lake, and the sediment pyrite abundance is <0.5 wt. % (Table 1).

The reduction of poorly crystalline Fe-oxyhydroxides and their subsequent stabilisation as more crystalline oxyhydroxide phases does exert major control over the fate of As in the present-day anoxic lacustrine system. In addition, percolation of anoxic waters into the porewater system appears to promote the leaching of weakly bound As stocks (Figure 2d). Hence, should the current ferruginous but not euxinic conditions prevail at the monimolimnion, the reductive dissolution of reducible Fe(III)-oxyhydroxide sinks has the potential to solubilise between 1.8 and 3.3 tons of As, i.e., by only considering the exchangeable and poorly crystalline oxyhydroxides fractions to a depth of 8 cm. These latent As levels would then accumulate in the monimolimnion to levels that represent an ecological risk.

Slight dissolved O_2 oscillations at the SWI observed during S_2 have proven to be instrumental for significant As remobilisation. More prevalent oxygenation of the bottom water column, such as in the event of holomixis, would thus increase the dissolved As concentrations of the monimolimnion to up to 0.73 mg L^{-1}, which would represent a 1.9-fold increase in its current average concentrations (i.e., 0.37 ± 0.17 mg L^{-1}, Appendix A, ST1). Currently, the monimolimnion's As concentrations are already considerably higher than the existing European thresholds for groundwater values (i.e., between 7.5 to 12 µg L^{-1}, Directive 2000/60/EC; European Community, 2000). In the foreseen transition to episodic holomixis, dissolved As levels would decrease to 27.7 µg L^{-1} in the entire water column, which would be 2-fold higher than the aforementioned thresholds.

Under anoxic (ferruginous) conditions the more mobile and toxic As(III) is expected to prevail (Smedley & Kinniburgh, 2002; Jiang et al., 2009). This is an environmental concern since As(III) can affect proteins and enzymes and thus, propitiate cell damage (Duker et al., 2005). The sediment's latent As concentrations can therefore be seen as an ecological risk to efforts to develop complex ecological networks such as ongoing fish introduction (e.g., Vejřík et al., 2017; Brázová et al., 2021) since the metalloid bioaccumulates in fish livers and gills (Kumari et al., 2017).

3.4.2 Latent sediment metal accumulations: economic secondary recovery feasibility

The fate of lanthanides in the sediment pile is governed by reactions transforming poorly crystalline Fe-oxyhydroxides (Figure 2e). Co-precipitation of REE with Fe into more crystalline oxyhydroxides appears to be a crucial process controlling the fraction-specific, lanthanide enrichment in our sediment pile. The enrichment of REE in the sediments would have initiated

even before the former mine was flooded, REE enrichment in the now anoxic lake sediments is up to 100 times higher than those measured in the Jozef creek (Figure 3b).

The REE-enriched sediments represent an outstanding secondary source of REE to the water column since their Post Archean Australian Shale (PAAS)-normalised concentrations are up to 10^4 times higher than those in the anoxic bottom waters (Figure 3b). Likewise, the REE content of the anoxic sediments in Medard is 10^6 times higher than the concentrations reported for seawater (Figure 3b) and is within the range observed in deep-sea sediments (e.g., Milinovic et al., 2021). These latter reservoirs have been considered as alternative yet still technologically challenging sources of REE (Milinovic et al., 2021).

Analogous to our calculations for As, but considering the total highly reactive pool, we estimate that the recent sediments (up to 8 cm depth) have REE contents that would become economically feasible. For example, considering that the recent upper anoxic sediment pile has accumulated 283 kg of Gd which at the time of writing has a price of 16,456 € kg^{-1}. Then, it could be estimated that the first 8 cm of the post-mining lake sediments contain a recoverable Gd accumulation with a value of up to 4.7M €. Similarly, the first 8 cm of these sediments contain a V accumulation equivalent to 7,730 kg, which at the current market price of 26.5 € kg^{-1} would have a value of 204k € should an 80% recovery efficiency be achieved. The figures given above can be expected to increase significantly due to a global supply shortage of such critical metals, increasing demand, a lack of substitutes, and mounting geopolitical pressures. Although these figures are broad and currently speculative, the calculations above highlight the possibility of developing post-mining lakes, such as Medard, as secondary sources of valuable metals.

An inexpensive and green alternative to recover such elements from solution is emerging in the increasing application of bioelectrochemical systems (BES) that use microorganisms as

biocatalysts to recover valuable dissolved resources efficiently and sustainably from wastewaters (Chatterjeea et al. 2019). BES can be optimised for high-efficiency metal removal and/or recovery (Wang & He, 2020), and the fundamentals behind a foreseen, economically feasible deployment of up-scaled BES in post-mining lakes are being actively investigated.

3.5 The fate of redox-sensitive metals as revealed by the REE systematics

We explored to what extent short-lived redox variations were recorded by the REE systematics of the Fe-rich lacustrine sediments under examination as a gauge for sediment transformation under suboxic conditions. As described in section 3.2.6 above, most REE (except for Ce) displayed lesser concentrations in S_2 (Table 2), which implies that the slightly increased redox potentials of the water column triggered lanthanides remobilisation (Figure 2e). Also, in S_1, the sediments below 2 cm, exhibited 3 times higher REE concentrations than the sediments near the SWI, which confirms the assertion above.

The average PAAS-normalised REE abundance patterns during both of the sampling periods are shown in Figure 4. The sediment REE content displayed a more variable behaviour in the uppermost sediment layers (black line, Figure 4a) than below this zone (grey shadowed line, Figure 4a). This implies that redox-sensitive metals – such as cerium – in recently deposited sediments are more prone to be influenced by minor shifts in the physicochemical conditions of the bottom waters. Also, the heavy rare earth elements (HREE) patterns from both sampling periods were similar, but the light rare earth elements (LREE) patterns varied. In S_1 (Figure 4a), an enrichment in LREE is consistent with La_N/Yb_N >1 (Appendix A, ST5). This LREE enrichment has been described as a signature of lignite weathering in other post-mining lake systems located in Central Europe (Bozau et al., 2004; 2008). Only LREE bonded to carbonates are depleted (i.e., La_N/Yb_N <1; Appendix A, ST5). This may be due to a stronger affinity of

carbonate towards HREE (Bozau et al., 2008; Laveuf & Cornu, 2009). An enrichment in the so-called MREE: i.e., Nd and Tb (Figure 4), is reflected by La_N/Sm_N ratios <1 (Appendix A, ST5). A similar MREE enrichment was also observed by Bozau et al. (2008) when studying other post-mining lakes more strongly influenced by acidic drainages.

Based on the variability of the abundance patterns of LREE between sampling periods, we evaluated the Ce and Eu anomalies, to determine if such variability corresponds to changes in the redox potentials of the overlying waters. The S_1 bulk sediment showed a negative Ce anomaly (Ce/Ce* range between 0.45 and 0.61 mean = 0.56; Appendix A, ST5) that is indicative of a relative depletion of Ce(III) (Figure 4a). This results from the reduction of Ce(IV) that solubilises trivalent Ce from the sediments (e.g., Haley et al., 2004). Under laboratory conditions, Nedel et al. (2010) demonstrated that cerium sorbed into easily reducible Fe(III)-oxyhydroxides and can be readily released into solution as the oxyhydroxides stabilise to more crystalline phases. In contrast, the Ce/Ce* values from S_2 ranged between 1.39 and 1.64 (mean = 1.53; Appendix A, ST5), and the PAAS-normalised REE abundance pattern (Figure 4b) depicted a positive Ce anomaly, which is likely related to the establishment of less reducing conditions in the SWI (Manoj & Kawsar, 2020) by the time of our 2020 sampling. Although the redox potential difference in the overlying water column was not so marked between sampling periods, and the SWI remained under suboxic conditions, the change in bottom water Eh that we recorded in S_2 appears to have been sufficient to stimulate further precipitation of poorly crystalline Fe(III)-oxyhydroxides while also favouring the oxidation of Ce(III) in solution and its subsequent immobilisation as Ce(IV) in the metastable mineral array of newly formed or altered phases (cf. Nedel et al., 2010).

We also evaluated the Eu anomaly, Eu/Eu*, but the values obtained in both sampling periods and for each fraction (mean = 0.1; Appendix A, ST5) indicates no occurrence of Eu anomalies in the sediment. Contrary to Ce, the observed changes in the environmental redox state were not sufficient to trigger Eu(III) release from Fe(III)-oxyhydroxide sinks nor its accumulation by co-precipitation within other mineral phases. This is not an unexpected result because europium could remain in solution as Eu(II) under circumneutral and highly reductive conditions. In this regard, it behaves as Fe(II) (MacRae et al., 1992; Tostevin et al., 2016). Besides, MacRae et al. (1992) estimated that detection of an Eu anomaly in recent sediments could be delayed by up to 10^3 years. Thus, the short-term redox variations targeted here do not produce significant changes in Eu speciation in the lacustrine sediment pile.

Relative enrichements of Ce are traditionally thought as a very sensitive proxy to minimal variability in O_2 levels in the water column (Tostevin et al., 2016). However, an environmental interpretation based on REE scatter plots alone could be inconclusive or lead to misinterpretations (Shields & Stille, 2001; Tostevin et al., 2016). For example, La enrichment in the system can lead to uncertainties in whether a Ce anomaly exist (Shields & Stille, 2001). Accordingly, a cross-plot of Pr/Pr* and Ce/Ce* values, as described by Bau & Dulski (1996), allowed us to confirm the occurrence of true negative (by S_1; Figure 5a), and true positive (by S_2; Figure 5b), Ce anomalies for all the reactive fractions, except for a few Ce_{CARB} and Ce_{RO} extractions from S_1 and S_2, respectively. These fractions, however, exert little control over the geochemical partitioning of Ce.

To conclude on the value of REE systematics as applied here, it effectively serves as a gauge for short-term variations in the monimolimnion's redox state and revels that, under suboxic conditions, transient shifts in the order of 100 mV are sufficient to propitiate significant changes

in speciation in redox-sensitive Ce but not Eu. These changes could then be extrapolated to occur for other redox-sensitive metal(loid)s of which speciation in the recent sediments evaluated here is linked to oxyhydroxide reactivity/crystallinity. Furthermore, should periodical redox state changes develop (e.g., seasonal holomixis), we determined that such changes would be swiftly recorded by the Ce anomaly of the sediments. Therefore, this parameter can be useful to gauge minor changes in the redox dynamics of the system and predict the behaviour of other metal(loid)s in lacustrine environments in general. This also applies to other post-mining lakes with similar hydrogeochemical features that could be the subject of economically feasible secondary recovery endeavours. Finally, the application of REE systematics also pinpoints the fact that oxygenation of the monimolimnion of post-mining lake systems could be relevant to the remobilisation of REE from the sediment pile to favour their technologically controlled scavenging from the water column, as discussed in section 3.4.

4. Conclusions

The post-mining Lake Medard acts as a large-scale incubation experiment, useful to further understand the evolution of aqueous mineral equilibrium as a response to drastic changes in redox state. Thus, the analysis of geochemical partitioning of redox-sensitive metal(loid)s with reactive Fe phases revealed that the sediments of this system have equilibrated to recently established bottom water anoxia but respond swiftly to transient shifts of the bottom water column towards a low-oxygen conditions. These shifts appear to be linked to change in salinity arising from seasonal hydrological variability. A sequential extraction protocol that targeted Fe mineral phases with diverse crystallinity and redox reactivity shows that As, V, and lanthanides are released from authigenic minerals formed under oxic conditions in the bottom of the former mine pit, with recycling of these elements likely occurring at the chemocline.

Accordingly, these elements are being immobilised anew either by their co-precipitation within Fe-oxyhydroxides of variable crystallinity or incorporation into Fe-carbonate phases distributed at a fluctuating abundance across the sediment pile.

Enrichment factors showed that the recent lacustrine sediments are moderately to acutely enrich in As, V, and lanthanides regarding world average and local backgrounds. The application of REE systematics to the post-mining lake sediment. It was also proven helpful to gauge the extent to which minor oscillations in the bottom water column's redox state produce significant changes in speciation of the redox-sensitive metal(loid)s evaluated here. Therefore, the approach applied here permits anticipating the fate of metals of interest (i.e., pollutants or critical transition metals) over potential variations of physicochemical parameters resulting from upcoming managing strategies. Predicting the evolution of the lacustrine sediment mineral equilibrium phases would be of great concern for potential management scenarios of the understudied post-mining lake. For example, a progressive mobilisation of labile As due to seasonal oxygenation of the water column would impede management scenarios involving the introduction of freshwater biota and thus, the establishment of complex ecological networks. Contrastingly, controlled scavenging of lanthanides and V by propitiating their co-precipitation in Fe mineral phases would make it plausible to consider post-mining lakes as secondary sources of critical transition metals.

Importantly, a sound understanding of the redox dynamics of lignite-derived post-mining lakes is not only relevant to the system under examination, but also to analogous anthropogenic environments numbers of which are expected to increase as coal-powered generation is being phased out. Similar to Lake Medard, some of these post-mining lakes might either represent an ecological risk due to their metalloids pollutants load or be amenable to secondary metal recovery endeavours. Therefore, results from this research could be applied to the decision-making process

of remediation and/or management programmes of post-mining lakes featuring similar hydrochemical and geological contexts.

Credit Authorship contribution statement

Conceptualisation: KU-S, AV, and DP; Lab Methodology: KU-S and AV; Field Methodology (i.e., specialised limnological sampling/monitoring): JJ and JB; Formal analysis: KU-S, AV and VC; Investigation: KU-S, AV, and DP; Resources: JJ, JB, DP and VC; Data curation: KU-S, AV and DP; Writing (original draft preparation): KU-S, AV and DP; Writing, review & editing: DP; Visualisation: KU-S; Supervision: DP; Project administration: DP; Funding acquisition: DP.

Declaration of competing interest

The authors declare that they have no competing financial interests or personal relationships that could influence their study.

Acknowledgements

This work was supported by the Czech Science Foundation, project no.19-15096Y. The authors are thankful to Stefan V. Lalonde for HR-ICP-MS analyses of the water samples.

References

Azcue, J. M., Nriagu, J. O., 1993. Arsenic forms in mine-polluted sediments of Moira Lake, Ontario. *Environ. Int.* 19 (4): 405-415. https://doi.org/10.1016/0160-4120(93)90131-Z.

Bau, M., Möller, P., 1993. Rare earth element systematics of the chemically precipitated component in early precambrian iron formations and the evolution of the terrestrial atmosphere-hydrosphere-lithosphere system. *Geochim. Cosmochim. Acta* 57 (10): 2239 – 2249. https://doi.org/10.1016/0016-7037(93)90566-F

Bau, M., Dulski, P., 1996. Distribution of yttrium and rare-earth elements in the Penge and Kuruman iron-formations, Transvaal Supergroup, South Africa. *Precambrian Res.*79 (1 – 2): 37 – 55. https://doi.org/10.1016/0301-9268(95)00087-9

Bethke, C. M., Farrell, B., Sharifi, M., 2021. GWB Reaction Modeling Guide. Aqueous Solutions LLC, IL USA. 1- 219. https://www.gwb.com/pdf/GWB2021/GWBrxnmodeling.pdf

Brázová, T., Šalamún, P., Miklisová, D., Šestinová, O., Findoráková, L., Hanzelová, V., Oros, M., 2021. Transfer of Heavy Metals Through Three Components: Sediments, Plants and Fish in the Area with Previous Mining Activity. *Bull. Environ. Contam. Toxicol*. 106:485–492. https://doi.org/10.1007/s00128-021-03114-w

Boehrer, B., Schultze, M., 2006. On the relevance of meromixis in mine pit lakes. *In:* Barnhisel RI (ed*) Proceedings, 7th international conference on acid rock drainage (ICARD),* St Louis, American Society of Mining and Reclamation: 200 – 213. http://dx.doi.org/10.21000/JASMR06020200

Boehrer, B., Schultze, M., 2008. Stratification of lakes. *Rev. Geophys.*46 (2): RG2005. https://doi.org/10.1029/2006RG000210

Bozau, E., Leblanc, M., Seidel, J.L., Stärk, H.-J., 2004. Light rare earth elements enrichment in an acidic mine lake (Lusatia, Germany). *J. Appl. Geochem.* 19 (3): 261 – 271. https://doi.org/10.1016/S0883-2927(03)00150-1

Bozau, E., Göttlicher J., Hans-Joachim S., 2008. Rare earth element fractionation during the precipitation and crystallisation of hydrous ferric oxides from anoxic lake water. *J. Appl. Geochem*. 23 (12): 3473 – 3486. https://doi.org/10.1016/j.apgeochem.2008.08.007

Canfield, D., Raiswell, R., Bottrell, S., 1992. The reactivity of sedimentary iron minerals toward sulfide. *Am. J. Sci* 292, 659–683. http://dx.doi.org/10.2475/ajs.292.9.659

Chatterjeea, P., Dessì, P., Kokko M., Lakaniemi, A-M., Lens, P., 2019. Selective enrichment of biocatalysts for bioelectrochemical systems: A critical review. *Renew. Sustain. Energy Rev.*109: 10 – 23. https://doi.org/10.1016/j.rser.2019.04.012

Czech Hydrometeorological Institute. Monthly sums of territorial precipitation from 1961 to 2021. Available online: https://www.chmi.cz/historicka-data/pocasi/uzemni-srazky?l=en (accessed on 08 June 2021).

Claff, S., Sullivan, L., Burton, E., Bush, R., 2010. A sequential extraction procedure for acid sulfate soils: partitioning of iron. *Geoderma* 155 (3 – 4): 224 – 230. https://doi.org/10.1016/j.geoderma.2009.12.002

Davison, W., 1993. Iron and manganese in lakes. *Earth-Sci. Rev.*34 (2), 119 – 163. https://doi.org/10.1016/0012-8252(93)90029-7

Dendievel, A.E., Mourier, B., Dabrin, A., Delile, H., Coynel A., Gosset, A., Liber, Y., Berger, J.F., Bedell, J.P., 2020. Metal pollution trajectories and mixture risk assessed by combining dated cores and subsurface sediments along a major European river (Rhône River, France). *Environ. Int.* 144: 106032. https://doi.org/10.1016/j.envint.2020.106032

Denimal, S., Bertrand, C., Mudry, J., Paquette Y., Hochart, M., Steinmann M., 2005. Evolution of the aqueous geochemistry of mine pit lakes –Blanzy–Montceau-les-Mines coal basin (Massif Central, France): origin of sulfate contents; effects of stratification on water quality. *J. Appl. Geochem.* 20 (5): 825 – 839. https://doi.org/10.1016/j.apgeochem.2004.11.015

Dixit, S., Hering, J., 2003. Comparison of arsenic(V) and arsenic(III) sorption onto iron oxide minerals: Implications for arsenic mobility. *Environ. Sci. Technol.*, 37 (18): 4182 – 4189. https://doi.org/10.1021/es030309t

Duker, A. A., Carranza, E.J.M., Hale M., 2005. Arsenic geochemistry and health. *Environ. Int.* 31 (5): 631-641. https://doi.org/10.1016/j.envint.2004.10.020.

European Community, 2000. Directive 2000/60/EC of the European Parliament and of the Council of 23 October 2000 establishing a framework for Community action in the field of water policy. *OJEC* 43, 1 – 72.

Gammons, C.H., Harris, L.N., Castro J.M., Cott, P.A., Hanna, B.W., 2009. Creating lakes from open pit mines: processes and considerations - with emphasis on northern environments. *Can. J. Fish. Aquat.* 2826: 106 p.

Haley, B.A., Klinkhammer, G.P., McManus, J., 2004. Rare earth elements in pore waters of marine sediments. *Geochim. Cosmochim. Acta* 68 (6): 1265 – 1279. https://doi.org/10.1016/j.gca.2003.09.012

Hannigan, R., Dorval, E., Jones, C., 2010. The rare earth element chemistry of estuarine surface sediments in the Chesapeake Bay. *Chem. Geol.* 272 (1 – 4): 20 – 30. https://doi.org/10.1016/j.chemgeo.2010.01.009

Hua J., Liu, C., Li, F., Zhu, Z., Wei, Z., Chen, M., Gao, T., Qiu, G., 2019. Effects of Rare Earth Elements' Physicochemical Properties on Their Stabilization during the Fe(II)aq-induced Phase Transformation of Ferrihydrite. *ACS Earth Space Chem.* 3 (6): 895 – 904. https://doi.org/10.1021/acsearthspacechem.8b00201

Jacob-Tatapu, K. J., Albert, S., Grinham, A., 2021. Sediment arsenic hotspots in an abandoned tailings storage facility, Gold Ridge Mine, Solomon Islands. *Chem.* 269: 128756. https://doi.org/10.1016/j.chemosphere.2020.128756

Jiang, J., Bauer, I., Paul, A., Kappler, A., 2009. Arsenic redox changes by microbially and chemically formed semiquinone radicals and hydroquinones in a humic substance model quinone. *Environ. Sci. Technol.* 43, 3639–3645. https://doi.org/10.1021/es803112a

Kontny, A., Schneider, M., Eiche, E., …, Neumann, T., 2021. Iron mineral transformations and their impact on As (im)mobilization at redox interfaces in As-contaminated aquifers. *Geochim. Cosmochim. Acta.* 296 (1): 189 – 209. https://doi.org/10.1016/j.gca.2020.12.029

Kříbek, B., Strand, M., Boháček, Z., Sýkorová, I., Čejkac, J., Sobalík, Z., 1998. Geochemistry of Miocene lacustrine sediments from the Sokolov Coal Basin (Czech Republic). *Int. J. Coal Geol.* 37 (3 – 4): 207 – 233. https://doi.org/10.1016/S0166-5162(98)00002-0

Kumari, B., Kumar, V., Sinha, A.K., Ahsan, J., Ghosh, A.K., Wang, H., DeBoeck, G., 2017. Toxicology of arsenic in fish and aquatic systems. *Environ. Chem.* 15: 43 – 64. https://doi.org/10.1007/s10311-016-0588-9

Laveuf, C., Cornu, S., 2009. A review on the potentiality of Rare Earth Elements to trace pedogenetic processes. *Geoderma* 154 (1 – 2): 1 – 12. https://doi.org/10.1016/j.geoderma.2009.10.002

MacRae, N.D., Nesbitt, H.W., Kronberg, B.I., 1992. Development of a positive Eu anomaly during diagenesis. *Earth Planet. Sci. Lett. 109* (3 – 54): 585 – 591. https://doi.org/10.1016/0012-821X(92)90116-D

Manoj, M.C., Kawsar, M., 2020. Metal contamination assessment in a sediment core from Vagamon Lake, southwest India: natural/anthropogenic impact. *Environ. Nanotechnol. Monit.* 14: 100362. https://doi.org/10.1016/j.enmm.2020.100362

Meyer, K.M., Kump, L.R., 2008. Oceanic euxinia in earth history: Causes and consequences. *Annu. Rev. Earth Planet. Sci.* 36 (1): 251 – 288. http://dx.doi.org/10.1146/annurev.earth.36.031207.124256

Milinovic, J., Rodrigues, F.J.L., Barriga, F.J.A.S, Murton, B. J., 2021. Ocean-floor sediments as a resource of Rare Earth Elements: An overview of recently studied sites. *Minerals* 11 (2): 142. https://doi.org/10.3390/min11020142

Murad, E., Rojík, P., 2003. Iron-rich precipitates in a mine drainage environment: Influence of pH on mineralogy. *Am. Mineral.* 88 (11-12): 1915 – 1918. http://dx.doi.org/10.2138/am-2003-11-1234

Murad, E., Rojík, P., 2005. Iron mineralogy of mine-drainage precipitates as environmental indicators: review of current concepts and a case study from the Sokolov Basin, Czech Republic. *Clays Clay Miner.* 40 (4): 427 – 440. http://dx.doi.org/10.1180/0009855054040181

Nance, W.B., Taylor, S.R., 1976. Rare earth elements patterns and crustal evolution – I. Australian post-Archean sedimentary rocks. *Geochim. Cosmochim. Acta.* 40 (12): 1539 – 1551. https://doi.org/10.1016/0016-7037(76)90093-4

Nealson, K.H., Belz, A., McKee, B.2002. Breathing metals as a way of life: geobiology in action. *Antonie van Leeuwenhoek* 81: 215 – 222. https://doi.org/10.1023/A:1020518818647

Nedel, S., Dideriksen, K., Christiansen, B.C., Bovet, N., Stipp, S.L.S., 2010. Uptake and release of cerium during Fe-oxide formation and transformation in Fe(II) solutions. *Environ. Sci. Technol.* 44 (12): 4493 – 4498. https://doi.org/10.1021/es9031503

Otchere, F.A., Veiga, M.M., Hinton, J.J., Farias, R.A., Hamaguchi, R., 2004. Transforming open mining pits into fish farms: Moving towards sustainability. *Nat. Resour. Forum* 28 (3): 216 – 223. https://doi.org/10.1111/j.1477-8947.2004.00091.x

Pačes, T., Šmejkal, V., 2004. Magmatic and fossil components of thermal and mineral waters in the Eger River continental rift (Bohemian massif, central Europe). *In:* R.B. Wanty and R.R.

Seal II (Eds.). Water-Rock Interaction. Taylor and Francis Group, London, AA. Balkema Publishers, ISBN 167-172.

Paikaray, S., Schröder, C., Peiffer, S., 2017. Schwertmannite stability in anoxic Fe(II)-rich aqueous solution. *Geochim. Cosmochim. Acta.* 217 (15): 292 – 305. https://doi.org/10.1016/j.gca.2017.08.026

Park, S., Lee, J-H., Shin, T.J., Hur, H-G., Kim, M.G., 2018. Adsorption and incorporation of arsenic to biogenic lepidocrocite formed in the presence of ferrous iron during denitrification by *Paracoccus denitrificans*. *Environ. Sci. Technol.* 52 (17): 9983 – 9991. https://doi.org/10.1021/acs.est.8b02101

Perez, J.P.H., Schiefler, A.A., Rubio, S.N., Reischer, M., Overheu, N.D., Benning, L.G., Tobler, D.J., 2021. Arsenic removal from natural groundwater using 'green rust': Solid phase stability and contaminant fate. *J. Hazard. Mater.* 401 (5): 123327. https://doi.org/10.1016/j.jhazmat.2020.123327

Petrash, D.A., Jan, J., Sirová, D., Osafo, N.O-A., Borovec, J., 2018. Iron and nitrogen cycling, bacterioplankton community composition and mineral transformations involving phosphorus stabilisation in the ferruginous hypolimnion of a post-mining lake. *Environ. Sci. Process Impacts* 20 (10): 1414 – 1426. https://doi.org/10.1039/C8EM00328A

Post, J., Bish, D., 1989. Rietveld refinement of crystal structures using powder X-ray diffraction data. *Rev. Mineral. Geochem.* 20 (1): 277 – 308. https://doi.org/10.1515/9781501509018-012

Poulton, S.W., Canfield, D.E., 2005. Development of a sequential extraction procedure for iron: implications for iron partitioning in continentally derived particulates. *Chem. Geol.* 214 (3 – 4): 209 – 221. https://doi.org/10.1016/j.chemgeo.2004.09.003

Raiswell, R., Canfield, D., 1996. Rates of reaction between silicate iron and dissolved sulfide in Peru Margin sediments. *Geochim. Cosmochim. Acta* 60, 2777–2788. https://doi.org/10.1016/0016-7037(96)00141-X

Sánchez-España, J., Yusta, I., Illin, A., van der Graaf, C., Sánchez-Andrea, I., 2020. Microbial Geochemistry of the Acidic Saline Pit Lake of Brunita Mine (La Unión, SE Spain). *Mine Water Environ.* 39: 535 – 555. https://doi.org/10.1007/s10230-020-00655-0

Shields, G., Stille, P., 2001. Diagenetic constraints on the use of cerium anomalies as palaeoseawater redox proxies: an isotopic and REE study of Cambrian phosphorites. *Chem. Geol.* 175 (1 – 2): 29 – 48. https://doi.org/10.1016/S0009-2541(00)00362-4

Schultze, M., Pokrandt, K-H., Hille, W., 2010. Pit lakes of the Central German lignite mining district: Creation, morphometry and water quality aspects. *Limnologica* 40 (2): 148 – 155. https://doi.org/10.1016/j.limno.2009.11.006

Schultze M., Boehrer B., Wendt-Potthoff K., Sánchez-España J., Castendyk D., 2017. Meromictic Pit Lakes: Case Studies from Spain, Germany and Canada and General Aspects of Management and Modelling. *In:* Gulati R., Zadereev E., Degermendzhi A. (eds) Ecology of Meromictic Lakes. Ecological Studies (Analysis and Synthesis), vol 228. Springer, Cham. https://doi.org/10.1007/978-3-319-49143-1_9

Smedley, P.L., Kinniburgh, D.G. A review of the source, behaviour and distribution of arsenic in natural waters. *J. Appl. Geochem.* 17 (5): 517 – 568. https://doi.org/10.1016/S0883-2927(02)00018-5

Sundman, A., Vitzthum, A-L., Adaktylos-surber, K., …, Byrne, J.M., 2020. Effect of Fe-metabolizing bacteria and humic substances on magnetite nanoparticle reactivity towards arsenic and chromium. *J. Hazard. Mater.* 384 (15): 121450. https://doi.org/10.1016/j.jhazmat.2019.121450

Tabelin, C.B., Corpuz, R.D., Igarashi, T., …, Hiroyoshi, N., 2020. Acid mine drainage formation and arsenic mobility under strongly acidic conditions: Importance of soluble phases, iron oxyhydroxides/oxides and nature of oxidation layer on pyrite. *J. Hazard. Mater.* 399 (15): 122844. https://doi.org/10.1016/j.jhazmat.2020.122844

Telfeyan, K., Breaux, A., Kim, J., Cable, J. E., Koller, A. S., Grimm, D. A., Johannesson, K. H., 2017. Arsenic, vanadium, iron, and manganese biogeochemistry in a deltaic wetland, southern Louisiana, USA. Mar. *Chem.* 192: 32 – 48. https://doi.org/10.1016/j.marchem.2017.03.010

Thompson, V. S., Gupta, M., Jin, H., 2017. Techno-economic and Life Cycle Analysis for Bioleaching Rare-Earth Elements from Waste Materials. *ACS Sustain. Chem. Eng.* 6 (2): 1602 – 1609. https://doi.org/10.1021/acssuschemeng.7b02771

Tostevin, R., Shields, G.A., Tarbuck, G.M., He, T., Clarkson, M.O., Wood, R.A., 2016. Effective use of cerium anomalies as a redox proxy in carbonate-dominated marine settings. *Chem. Geol.* 438 (2): 146 – 162. https://doi.org/10.1016/j.chemgeo.2016.06.027

Turekian, K.K., Wedepohl, K.H., 1961. Distribution of the elements in some major units of the earth's crust. *Geol. Soc. Am. Bull.* 72 (2): 175 – 192. https://dx.doi.org/10.1130/0016-7606(1961)72[175:DOTEIS]2.0.CO;2

van de Velde, S.J., Reinhard, C.T., Ridgwell, A., Meysman, F.J.R., 2021. Bistability in the redox chemistry of sediments and oceans. *Proc. Natl. Acad. Sci. U. S. A.* 117, 33043–33050. https://doi.org/10.1073/PNAS.2008235117

Vejřík, L., Vejříkova, I., Blabolil, P., …, Čech, M., 2017. European catfish (*Silurus glanis*) as a freshwater apex predator drives ecosystem via its diet adaptability. *Sci. Rep.* 7: 15970. https://www.nature.com/articles/s41598-017-16169-9

Wang, Z., He, Z., 2020. Frontier review on metal removal in bioelectrochemical systems: mechanisms, performance, and perspectives. *J. Hazard. Mater. Letters* 1: 100002. https://doi.org/10.1016/j.hazl.2020.100002

Wang, M., Wu, S., Guo, J., Liao, Z., Yang, Y., Chen, F., Zhu, R., 2021. Immobilization and migration of arsenic during the conversion of microbially induced calcium carbonate to hydroxylapatite. *J. Hazard. Mater.* 412: 125261. https://doi.org/10.1016/j.jhazmat.2021.125261

Woon, S. H. J., Srinuansom, K., Chuah, C. J., Ramchunder, S. J., Promya, J., Ziegler, A. D., 2021. Pre-closure assessment of elevated arsenic and other potential environmental constraints to developing aquaculture and fisheries: The case of the Mae Moh mine and power plant, Lampang, Thailand. *Chem.* 269: 128682. https://doi.org/10.1016/j.chemosphere.2020.128682

Zhang, C., Yu, Z-G., Zeng, G-M., …, Hu, L., 2014. Effects of sediment geochemical properties on heavy metal bioavailability. *Environ. Int.* 73: 270 – 281. https://doi.org/10.1016/j.envint.2014.08.010

- **Figure 1.** Lake Medard (Karlovy Vary region, NW Czech Republic). Brown areas indicate the current deepest and permanently anoxic sedimentary basins of the lake. "S" indicates the central sampling location. Satellite imagery was extracted from Google Earth® in June 2021.

- **Figure 2.** Depth metal concentration profiles of highly reactive fractions in the lacustrine sediments of Lake Medard. The upper part shows concentration values corresponding to the first sampling (S_1; November 2019), while the lower part corresponds to the second sampling (S_2; December 2020). Colour/sampling codes as in Fig. 1

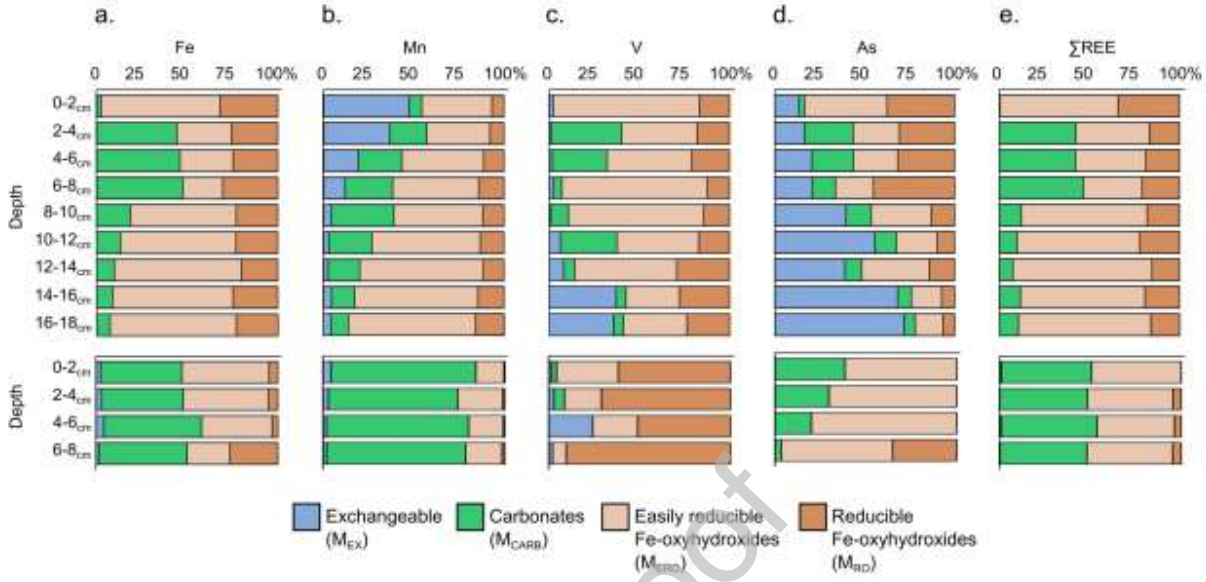

- **Figure 3.** Relative enrichment in the post-mining lacustrine sediment profiles, using the mean values between both sampling periods, and considering the average concentration from the core. The figure shows (a) the calculated enrichment factor (EF, Eq. 4) normalising the total concentrations of the highly reactive (M_{HR}) pool with regard to: (i) world average carbonate (WAC, ●; Turekian & Wedepohl, 1961); (ii) shale (WAS, ○; Turekian & Wedepohl, 1961); and (iii) the local claystone lithology of the Sokolov basin (Miocene Cypris Fm., ▲; Kříbek et al. 1998), and (b) the Post-Archean Australian shale (PAAS) REE abundance patterns by the S_1 ●[OB] and S_2 ○[OB] sampling. For comparison purposes, we also plotted the PAAS-normalised patterns of the O_2-depleted water column (monimolimnion +[OB]; and the acidic drainage (JC ■[OB]). See text for details.

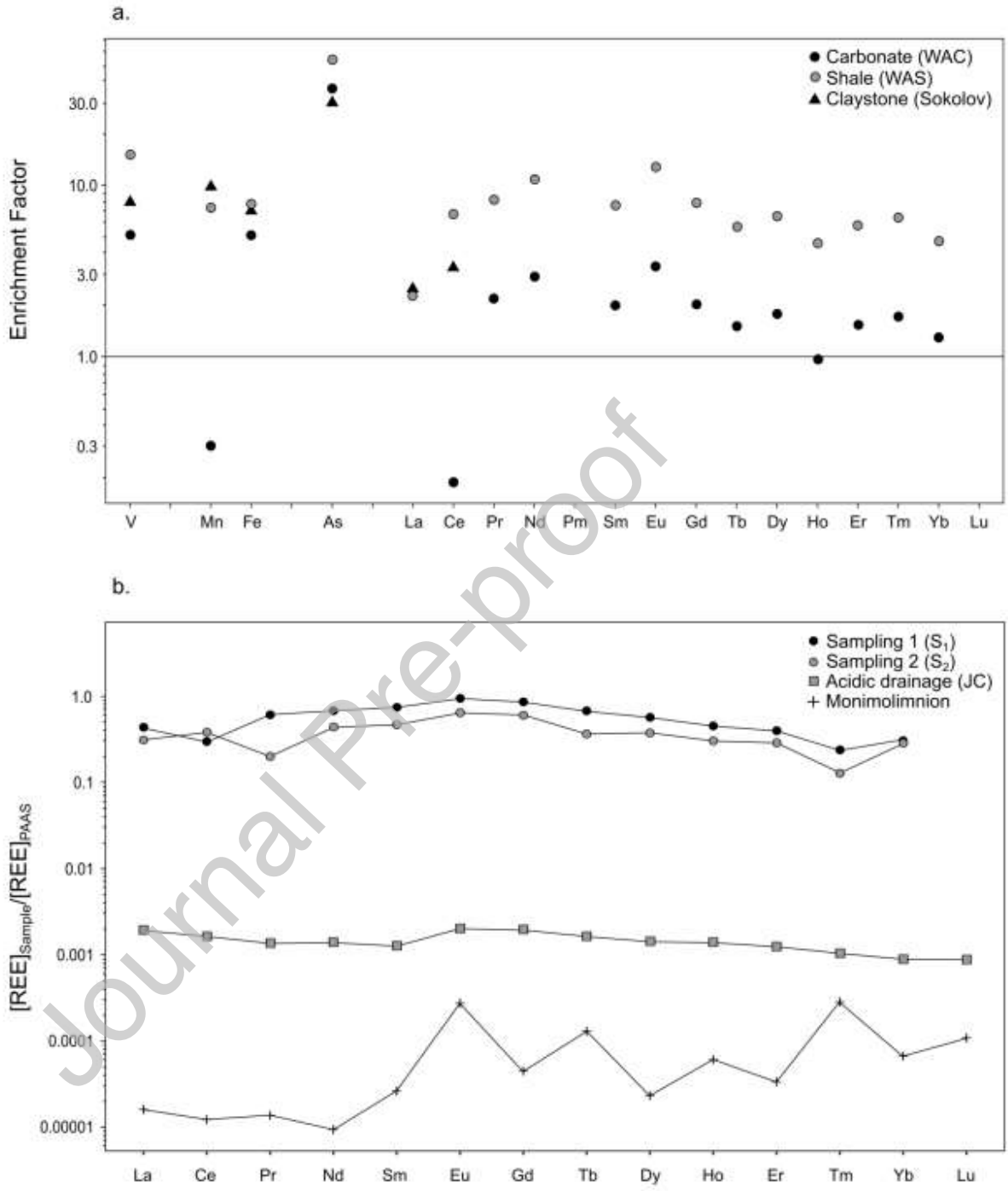

- **Figure 4.** Scatter plot displaying the average PAAS-normalised REE abundance patterns of sediments collected in (a) $S_{1;}$ and (b) S_2. Black line indicates the obtained pattern by using concentrations from 0-2 cm depth by S1(●), and from 2 to 18 cm depth by S_1 and 0 to 18 cm depth by S_2 (●), with the grey shadow portraying the range of average concentrations.

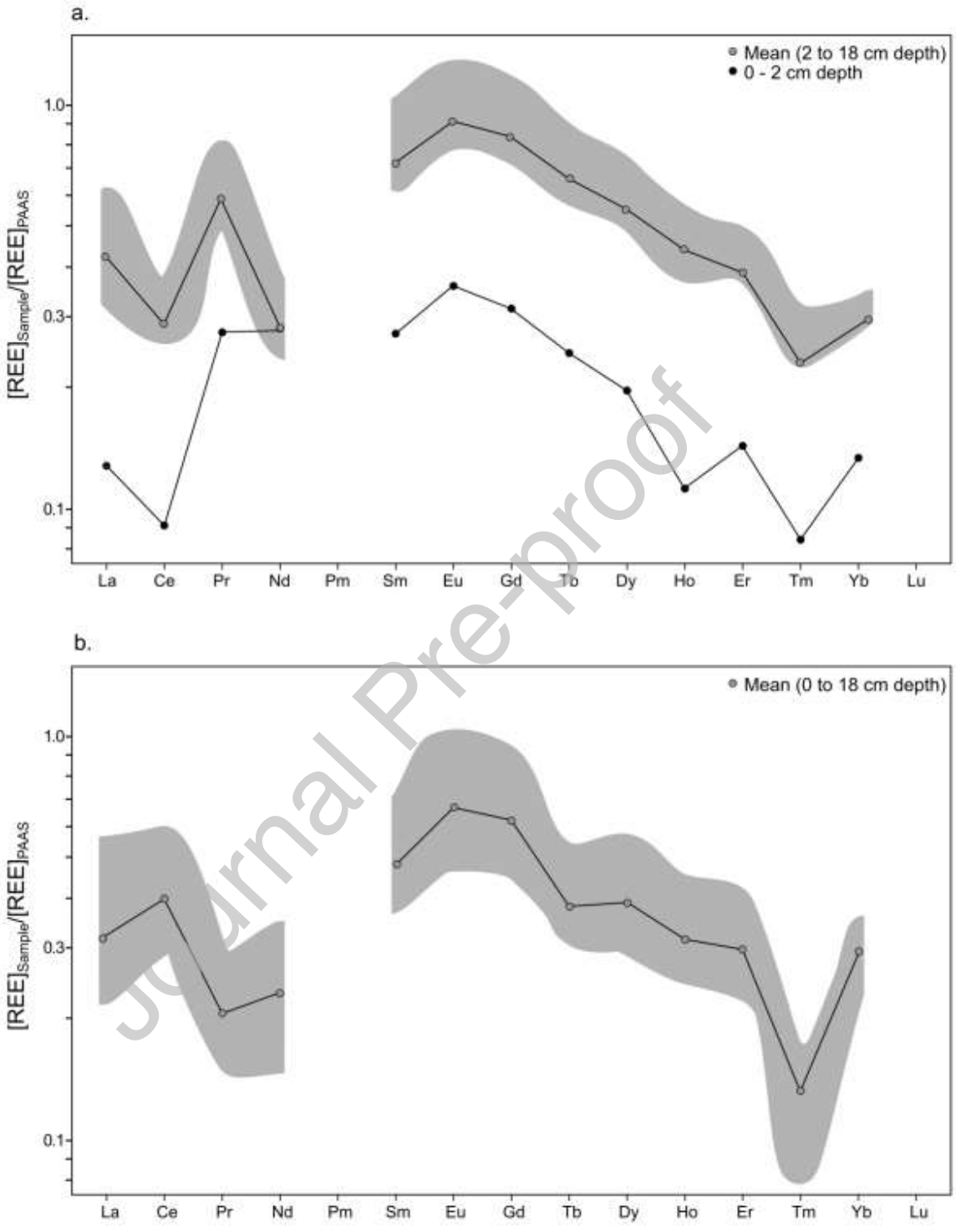

- **Figure 5.** PAAS-normalised Ce/Ce^{*} *vs.* Pr/Pr^{*} cross-plot. The diagram helps in elucidating whether true La and Ce anomalies exist in the discrete reactive phases evaluated here. Colour/sampling codes as in Fig. 1.

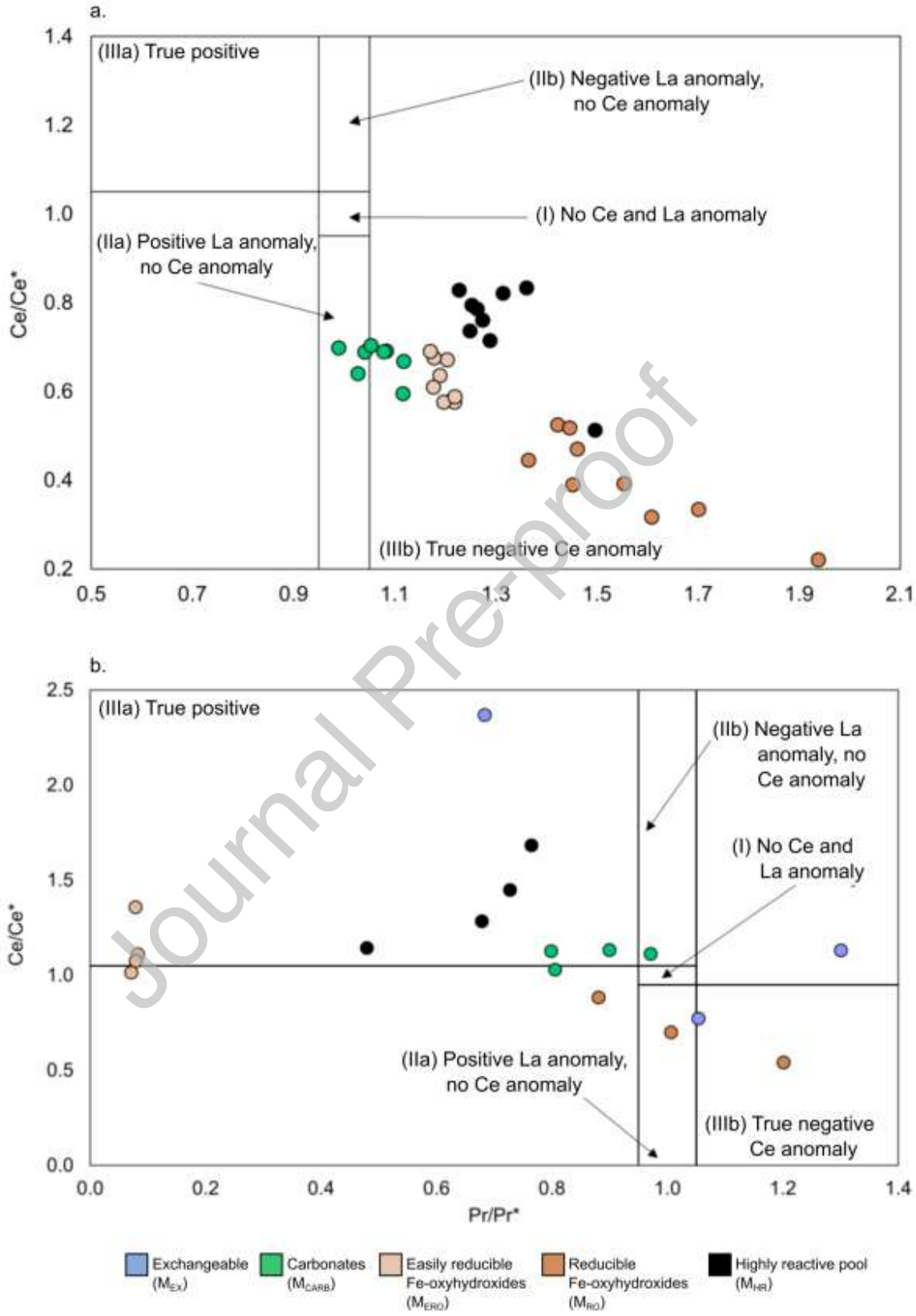

Table 1. Concentration values of TOC, TN contents, and C/N ratios. In the upper part we listed the values corresponding to the first sampling (S_1; November 2019); while the lower part corresponds to the second period (S_2; December 2020). The range of semi-quantitative (XRD) mineralogical abundances in the sediments is also listed.

Sampling	Depth (cm)	TOC (%)	TN (%)	C/N
S_1	**0-2**	5.13	0.31	16.55
	2-4	3.93	0.20	19.65
	4-6	3.73	0.19	19.63
	6-8	3.70	0.17	21.76
	8-10	1.36	0.04	34.00
	10-12	1.34	0.03	44.67
	12-14	4.29	0.05	85.80
	14-16	1.73	0.03	57.67
	16-18	1.57	0.02	78.50
S_2	**0-2**	4.69	0.28	16.88
	2-4	3.93	0.23	17.17
	4-6	3.68	0.22	16.62
	6-8	4.09	0.14	29.28

Semi-quantitative phase analysis (range wt.%): kaolinite 66.0 - 68.5, quartz 8.0 - 9.0, mica 2.0 - 3.0, plagioclase 1.0 - 2.5, K-feldspar 3.0 - 6.0, gypsum 2.5 - 3.5, anatase 5.0 - 5.5, rutile 0.5 -1.0, analcime 1.0 - 2.0, siderite 2.0 - 3.0, pyroxene 3.0

Variability (%): TOC = 0.21 (S_1), 0.37 (S_2); TN = 0.02 (S_1), 0.05% (S_2)

Table 2. Total elemental concentration (in $mg \cdot kg^{-1}$) of the highly reactive pool of metal(loid)s extracted in both sampling periods.

Sampling	Depth (cm)	Al	Fe	Mn	V	As	La	Ce	Pr	Nd	Sm	Eu	Gd	Tb	Dy	Ho	Er	Tm	Yb	ΣREE
S_1	**0-2**	5011.6	14228.1	402.2	69.9	49.4	4.9	7.3	2.4	8.9	1.5	0.4	1.5	0.2	0.9	0.1	0.4	0.04	0.4	28.9
	2-4	8276.6	26377.2	362.5	110.9	64.9	13.3	19.9	4.2	16.8	3.2	0.8	3.3	0.4	2.1	0.4	0.5	0.1	0.9	66.5
	4-6	9573.7	26947.1	250.5	98.8	61.2	13.9	21.6	4.9	19.5	3.5	1.0	3.6	0.5	2.4	0.4	0.5	0.1	0.9	73.4
	6-8	9961.8	51295.3	314.8	145.8	123.8	23.9	29.6	6.0	23.5	4.1	1.2	4.5	0.6	2.9	0.6	0.6	0.2	1.1	99.7
	8-10	4162.8	11978.3	299.7	120.2	41.2	15.2	23.5	5.2	21.2	4.4	1.0	4.1	0.5	2.7	0.5	1.1	0.1	0.9	80.5
	10-12	2874.1	12197.3	353.2	63.8	45.2	17.6	23.3	5.2	21.1	4.2	1.0	3.9	0.5	2.4	0.4	0.9	0.1	0.8	81.5
	12-14	3177.8	14494.8	380.1	51.6	45.4	21.0	30.0	7.3	29.8	5.9	1.4	5.5	0.7	3.2	0.6	1.3	0.1	1.0	108.0

	14-16	387 4.1	1206 2.3	30 5.9	68. 7	59. 4	17 .1	25 .6	5. 9	24 .5	4. 7	1. 2	4. 6	0. 6	2. 7	0. 5	1. 0	0. 1	0. 8	89. 6
	16-18	373 1.2	1302 2.6	34 0.1	71. 7	63. 8	18 .2	26 .4	6. 0	24 .2	4. 7	1. 2	4. 4	0. 6	2. 6	0. 5	0. 9	0. 1	0. 8	90. 8
S_2	**0-2**	412 0.3	2186 2.5	80 9.2	11 0.2	37. 5	8. 1	22 .9	1. 3	10 .4	2. 0	0. 5	2. 1	0. 2	1. 3	0. 2	0. 7	0. 1	0. 6	50. 4
	2-4	469 8.2	2279 7.2	45 2.1	17 3.6	25. 9	8. 1	25 .8	1. 6	12 .0	2. 3	0. 6	2. 4	0. 2	1. 5	0. 3	0. 7	0. 0	0. 7	56. 3
	4-6	382 4.1	2356 7.3	50 4.6	93. 2	20. 1	10 .6	27 .8	1. 6	12 .8	2. 3	0. 6	2. 5	0. 3	1. 6	0. 3	0. 8	0. 0	0. 8	62. 2
	6-8	763 1.3	4936 4.8	32 3.0	38 3.5	55. 8	21 .0	47 .1	2. 6	21 .7	4. 0	1. 1	4. 3	0. 4	2. 4	0. 4	1. 1	0. 1	1. 1	107 .3

Variability range (%) (S_1 and S_2): Al, V, Mn, Fe = [4.4 to 9.0]; As = [8.3 to 10.6]; REE = [1.5 to 10.8**]**